Numerical model for granular compaction under vertical tapping

P. Philippe and D. Bideau
GMCM, Bâtiment 11A, Campus de Beaulieu, Université de Rennes I, F-35042 Rennes, France
(Received 27 November 2000; published 20 April 2001)

A simple numerical model is used to simulate the effect of vertical taps on a packing of monodisperse hard spheres. Our results are in good agreement with an experimental work done in Chicago and with other previous models, especially concerning the dynamics of the compaction, the influence of the excitation strength on the compaction efficiency, and some aging effects. The principal asset of the model is that it allows a local analysis of the packings. Vertical and transverse density profiles are used, as well as size and volume distributions of the pores. An interesting result concerns the appearance of a vertical gradient in the density profiles during compaction. Furthermore, the volume distribution of the pores suggests that the smallest pores, ranging in size between tetrahedral and octahedral sites, are not strongly affected by the tapping process, in contrast to the largest pores which are more sensitive to the compaction of the packing.

DOI: 10.1103/PhysRevE.63.051304 PACS number(s): 45.05.+x, 45.70.Cc, 61.20.−p, 81.05.Rm

I. INTRODUCTION

Granular materials constitute the raw materials in a huge number of human activities such as agriculture, the mining industry, and pharmaceuticals, and are at the heart of the matter in several ecological challenges such as avalanches or desertification by eolian erosion. Therefore, explaining a few current granular processes, such as storage, transport, or collapse, is a real economical challenge. Furthermore, packings of spheres, which comprise the simplest model of a granular medium, have a great fundamental interest for physicists: hard sphere systems are indeed a common description of simple liquids [1]; moreover grains can behave, according to the external conditions, more or less like a solid, a liquid, or a gas [2]. This great variety of behaviors for a banal heap of grains makes granular mechanics a rich area of investigation, only partially clarified at the moment. It is now a well-known result [3–5] (although there is no theoretical explanation for it) that a disordered static packing of equal hard spheres can cover a large range of volume fractions, approximately from 56%, for random loose packing, to 64%, for random close packing (R.C.P.). For a regular arrangement, the packing fraction can reach up to 74% which corresponds to the densest structures, namely the hexagonal compact (H.C.) and the face-centered-cubic (fcc) crystals.

The thermal energy (k_BT) plays no role, because it is insignificant compared to the gravitational energy of a macroscopic grain; each packing of spheres is a metastable configuration which can persist as long as there is no external excitation. In this framework, issues of the compaction of grains under vertical taps are a practical way to study the succession of jumps from a metastable equilibrium to another one. The initial packing is quite loose, and can progressively reach a nearly stationary configuration (steady state) evaluated through its average volume fraction. Some experiments done in Chicago [6–8] studied the influence of the tapping intensity on the steady-state value and the dynamics of the compaction, which is approximately the inverse of the logarithm of the number of taps. The experimental setup is a thin tube of diameter $D=1.88$ cm, filled to about an 80-cm height with monodisperse, spherical soda-lime glass beads (of diameter $d=1$, 2, or 3 mm). The tube is shaken by an electromagnetic exciter delivering vertical taps, each consisting of an entire cycle of a sine wave of frequency $f=30$ Hz. The excitation strength is parametrized by Γ, the ratio between the measured acceleration peak and the gravitational acceleration g. Moreover, several numerical and theoretical works [9–15], most of them dealing with notions of free volume and geometric constraint, found the same kind of behavior as obtained experimentally; some of them [10,11] pointed out structural aging effects, as typically observed in glassy systems. Thus a parallel might exist between this granular compaction and the dynamics of out-of-equilibrium systems like glasses.

In this work, we used a simple model to simulate the compaction of a packing of monosize spheres submitted to vertical taps. We did not try to make a realistic description of the quite complex succession of collisions in a shaken packing: as the only ingredient of the model we retained a geometric constraint between hard spheres, which is believed to be the principal origin of the compaction. Despite the fact that we deliberately omitted the mechanical dimension of the problem, the model is able to reproduce qualitatively the experimental results of the Chicago group, as well as some further results in agreement with different numerical and theoretical studies. As the model seems to capture the physics of the problem, it is then possible to go beyond a global analysis. Indeed, as a three-dimensional packing of hard spheres, our description has the quite interesting asset that it is very close to a real granular medium. Thus, contrary to almost all previous works which dealt only with a macroscopic probe (i.e., the average density in all or part of the packing), our model can provide us with realistic information about the local structure of a packing and its evolution under compaction by taps.

This paper is organized as follows. A detailed description of the model is presented in Sec. II. Section III is devoted to a global analysis of compaction (logarithmic dynamics, hysteresis effect, and aging behaviors). In Sec. IV, the local analysis of the packings is described with the use of density profiles and size and volume distributions of the pores. Our conclusions and perspectives end the paper in Sec. V.

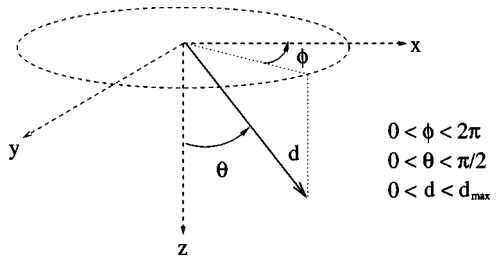

FIG. 1. A typical displacement during the redeposition stage of the algorithm.

II. MODEL

The model proposed here is purely geometric, and deals only with the steric constraint, neither friction nor contact law between the spheres or with the walls is introduced. The different sequences of tapping were initialized from a relatively loose packing obtained by a steepest-descent algorithm, simulating a sequential gravitational deposition [16]. We worked with packings of 4096 spheres of radius R piled up in a square-box of dimension $L=32R$. Concerning the vertical walls, we used both periodic boundary conditions (P.B.C.'s) and fixed boundary conditions (F.B.C.'s) i.e. impassable vertical planes. The top of the box is open, whereas the bottom is a fixed impassable plane.

A tap is decomposed in two stages: first a vertical dilation and then a gravitational redeposition.

The first stage corresponds to an external excitation, which will enable the packing to move from a metastable equilibrium to another one. We used the simplest way to simulate the tap by applying a uniform dilation ε to the whole packing $[z \rightarrow z(1+\varepsilon)]$. This reduction is certainly far from a real tap, but we assume that the way of dilating the packing is less important than the result of the dilation: a significant increase of the average free volume of the spheres will allow collective rearrangements during the second stage—the redeposition of the packing.

This redeposition procedure must be nonsequential in order to permit such collective behaviors; thus we use a Monte Carlo algorithm to discretize the motion of the spheres: a great number of small displacements is computed. An individual movement procedure is structured as follows: a sphere, randomly chosen, is submitted to a small random displacement; if this displacement creates no interpenetration with another sphere or with the walls (according to the boundary conditions), it is accepted; otherwise it is rejected. Because of this binary schema, two neighboring spheres cannot be exactly in contact but, after a sufficient time, they become very close to contact. Figure 1 shows a typical displacement: the values of the polar angle ϕ and the displacement d are strictly randomly chosen between 0 and 2π and 0 and d_{max}, respectively, whereas the choice of the angle θ follows a random distribution centered on zero to mimic the effect of gravity. We use the following Gaussian distribution of width θ_0 truncated beyond $\pi/2$ in order to orientate all the displacements down to the bottom of the box:

$$P(\theta)=A\exp[-(\theta/\theta_0)^2]. \tag{1}$$

The choice of the distribution does not seem to be restrictive: some attempts with a Poissonian distribution and a linear distribution gave qualitatively the same phenomenology: the pertinent parameter is the width θ_0.

With such an algorithm, agitation will persist indefinitely. So we regularly test the packing during the redeposition process. The variable checked is $\langle Z \rangle$, the average altitude of the packing that is the average potential energy of the spheres. The redeposition is stopped when the relative variation of $\langle Z \rangle$ becomes smaller than a threshold η. The choice of $\langle Z \rangle$ is motivated by its easy evaluation during the process, and by its possible link with a statistical mechanics approach.

This simulation is rather close to the one proposed by Barker and Mehta [17] but with some differences, especially concerning the way of introducing gravity and the end of the redeposition stage.

The model uses four parameters: d_{max}, η, θ_0, and ε. The first two have a direct effect on the simulation time. The smaller the value of η, the longer the simulation time; still, η must be small enough if we want the redeposition to be nearly completed. The parameter d_{max} has to be optimized. A very small value of d_{max} allows almost all of the displacements to be accepted, but the effect on the redeposition is very slight and the packing is therefore nearly frozen. Conversely, for a large value of d_{max}, almost all the displacements are refused and, once again, the packing evolves very slowly. In this study, we used the intermediate value $d_{max}=\mathrm{R}/5$.

θ_0 has a significant effect on the packing behavior: a very small θ_0 induces a decompaction, whereas a large value decreases the efficiency of the compaction. We found $\theta_0=\pi/4$ as the optimized value, giving rise to the maximal compaction rate.

The last parameter ε corresponds to the external excitation induced in the packing. This is our control parameter. The value of ε can be estimated from experimental results concerning the dilation of a vertically shaken sand heap [18]: $\varepsilon=\delta h/h\approx 5/500\approx 10^{-2}$. We can also try to link ε roughly to the experimental control parameter, the dimensionless acceleration $\Gamma=A\omega^2/g$ where A and ω are, respectively, the amplitude and the frequency imposed on the bottom of the heap. In a first approximation, if we neglect the loss of energy in the packing, a particle at the top of the heap $[z(0)=h]$ acquires an initial speed ωA and achieves a ballistic flight. Its maximal altitude is $z(0^+)=h+(g/2)(\Gamma/\omega)^2$, and then

$$\Gamma=\omega\left(\frac{2h}{g}\right)^{1/2}\varepsilon^{1/2}\Rightarrow\Gamma\propto\varepsilon^{1/2}. \tag{2}$$

As $\varepsilon^{1/2}$ is linked to Γ, we will use it as our control parameter to quantify the strength of the tapping process. With this, it is possible to compare the results of our model with the experimental work of the Chicago group and with other numerical and theoretical models, almost all of them dealing only with a global description of the granular system.

III. GLOBAL ANALYSIS

This global analysis is achieved with different average values. We did not use a direct evaluation of the packing

fraction from the number of spheres in a reference volume because, whether boundary effects are significant or, for a smaller volume, the statistics become too poor. Moreover, the choice of the reference volume is not unique: it can be, for example, the space that contains all the spheres, or a smaller space that contains only the centers of the spheres. To avoid being partial, we evaluate the packing fraction by averaging the surface packing fraction Φ, calculated on many horizontal cuts. This measure is permissible because of the following stereologic result: the average surface fraction of any cut in a packing is equal to the volume fraction of the packing [19]; with horizontal cuts, this calculus is just a spatial integration which gives the exact volume fraction. The quantity Φ_b is calculated in this way at the bottom of the packing between the heights 0 and $4R$; $\langle \Phi^c \rangle$ comes from a similar calculation on approximately 90% of the packing, and is corrected near the bottom wall by a perturbated zone model [20]. This model uses a corrective factor for the average density of a packing near a wall (between 0 and R) with regard to a packing not perturbated by any wall. For the case of spheres near a plane, this factor is estimated to 16/11. It is also interesting to study $\langle Z \rangle$, the average potential energy of the whole system, which is quite pertinent in a statistical mechanics description.

A. Dynamics of compaction

The densification of the packing is observed through the temporal evolution of the preceding mean values; here the time is the number of taps, and what we call the dynamics of the compaction is, in fact, the succession of metastable equilibrium, each jump from one to another being induced by the taps. Figure 2 shows compaction laws obtained with fixed boundaries (F.B.C.'s) and three different excitation rates. This excitation intensity $\varepsilon^{1/2}$ has a decided effect on the compaction dynamics (see Sec. III B). The simulation curves are in good agreement with the experimental data and compatible with the following fit previously proposed [6],

$$X(t) = X_\infty - \frac{\Delta X_\infty}{1 + B_X \ln(1 + t/\tau_X)}, \tag{3}$$

with $X = \Phi_b$ or $\langle \Phi^c \rangle$. For $\langle Z \rangle$, a nearly similar fit can be proposed:

$$\langle Z \rangle(t) = \langle Z \rangle_\infty \left(\frac{1 + B_Z \ln(1 + t/\tau_Z)}{\frac{\langle Z \rangle_\infty}{\langle Z \rangle_0} + B_Z \ln(1 + t/\tau_Z)} \right). \tag{4}$$

We have noted that a sum of two exponentials can also fit $\langle Z \rangle(t)$ reasonably well.

The dependence of these parameters on ε is difficult to characterize. We simply note that the parameter B is consistent with an exponential dependence on $\varepsilon^{1/2}$ (i.e., Γ).

This compaction dynamics is quite particular: as the packing progressively densifies, the compaction efficiency decreases. Thus the dynamics reduces its speed, and the system evolves to a steady state without ever really reaching the state. This slowing down is particularly remarkable for the smallest values of $\varepsilon^{1/2}$. This specific dynamics requires the study of the densification on a logarithmic time scale.

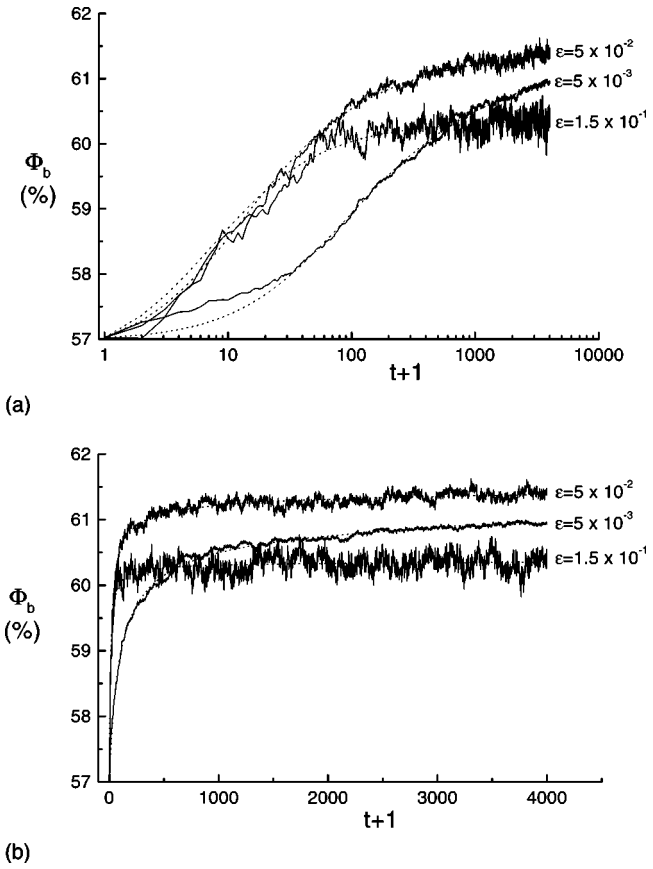

FIG. 2. Bottom packing fraction Φ_b vs t, the number of taps, on logarithmic (up) and linear (down) time scales for three excitation rates ($\varepsilon = 5\times10^{-3}$, 5×10^{-2}, and 1.5×10^{-1}). The solid lines are the simulation results, and the dotted lines are the inverse-logarithmic fits.

It is also interesting to analyze the fluctuations of the curves, especially when the packing becomes close to its asymptotic or steady-state limit. The power spectrum of the fluctuations $X - X_{SS}$ as a function of the frequency, i.e., the inverse of the tap number, shows more or less a simple power law in a log-log diagram (with a slope in the range 1–1.5). The effect of ε is noticable only for the high frequencies. Moreover, the simple standard deviation of the fluctuations, $\sigma_X = \sqrt{\langle (X - X_{SS})^2 \rangle}$, seems to be directly proportional to $\varepsilon^{1/2}$ or Γ. These results, calculated for $X = \langle Z \rangle$, are presented in Fig. 3. Furthermore, we have noted that the periodic boundary conditions do not qualitatively affect these observations; the same remark can be made concerning the results of Sec. III B.

B. Hysteresis on the steady-state values

The next stage consists of studying the influence of the excitation parameter $\varepsilon^{1/2}$ on the maximal value of the packing fraction. For this purpose, we carried out a succession of simulations with a sequence of 4000 taps. The steady-state value is estimated by averaging the packing fraction on the 1000 last taps, or directly through the last value. The smaller

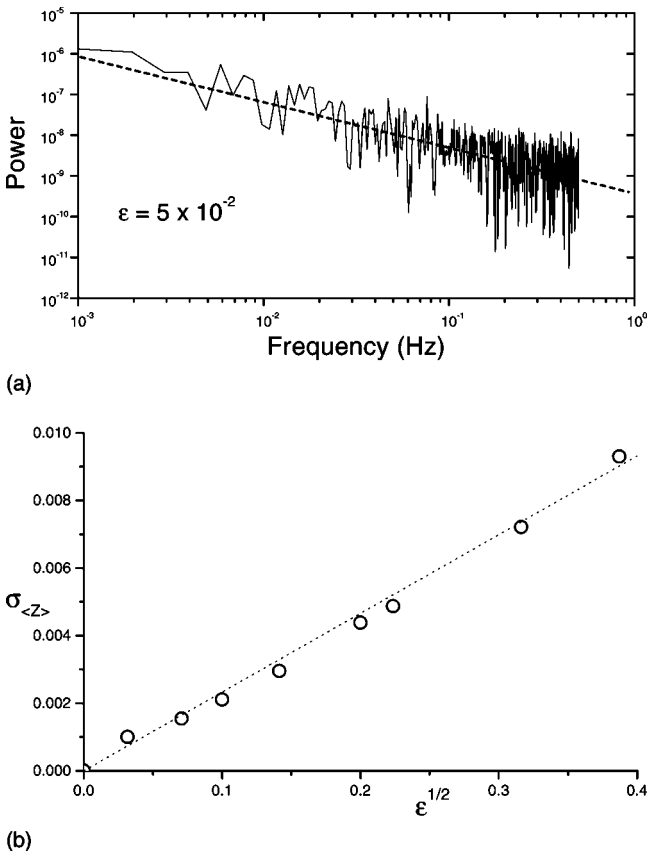

FIG. 3. The power spectrum of the fluctuations of $\langle Z\rangle$ vs frequency (the inverse of the number of taps) (up) and the simple standard deviation of $\langle Z\rangle$, $\sigma_{\langle Z\rangle}$, which is nearly linear with $\varepsilon^{1/2}$ (down).

$\varepsilon^{1/2}$ is, the larger the difference between this steady-state value and the asymptotic value X_∞ given by the fit. Moreover, in this small excitations range, X_∞ can overcome the R.C.P. limit, and τ, the characteristic time of the fit, increases spectacularly. In fact, the fit becomes more and more uncertain in so far as the triplet (X_∞, B, τ) is no longer unique, and depends strongly on the range of taps over which the data fitting is performed. This deviation between the steady-state value and an uncertain asymptotic limit was also noted in the experimental work of the Chicago group [8] and in some theoretical studies [13,15]. The dependence of $\langle\Phi^c\rangle$ on $\varepsilon^{1/2}$ is shown in Fig. 4 (solid black squares). The different packings are obtained after 4000 taps of strength ε, starting from the same initial packing. The curve has a bell shape with a maximum between 0.1 and 0.2.

If we now compute a unique tapping sequence with a progressive increase of the excitation $\varepsilon^{1/2}$ after every 4000 taps (the constant excitation increment is $\Delta\varepsilon^{1/2}=+0.025$), we obtain nearly the same curve for $\langle\Phi^c\rangle$, as can be seen in Fig. 4 (open circles). When carrying out the same process in the opposite way, i.e., with a progressive decrease of $\varepsilon^{1/2}$ ($\Delta\varepsilon^{1/2}=-0.025$), two things can happen.

If, while increasing, $\varepsilon^{1/2}$ goes beyond a critical value of $(\varepsilon^{1/2})^*\approx 0.15$, the final packing fraction $\langle\Phi^c\rangle$ does not decrease but increases a bit more to a maximum value. If we compute another increase process ($\Delta\varepsilon^{1/2}=+0.025$), we

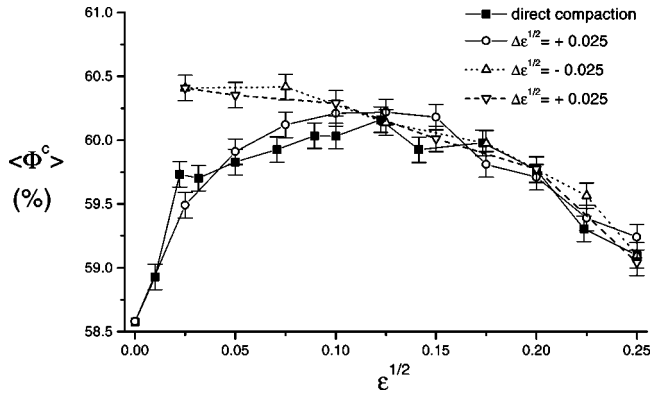

FIG. 4. Steady-state values of $\langle\Phi^c\rangle$ obtained after 4000 taps with different values of $\varepsilon^{1/2}$ (solid black squares) and hysteresis during a sequence of increase (open circles), decrease (open up triangles) and increase (open down triangles) of the excitation with an increment $\Delta\varepsilon^{1/2}$ every 4000 taps.

cover approximately the same values. This last upper branch, including the part above $(\varepsilon^{1/2})^*$ is represented in Fig. 4 (up and down open triangles). As it is relatively well reproducible, it is called ''reversible.'' We can also see on this reversible branch that $\langle\Phi^c\rangle$ decreases with $\varepsilon^{1/2}$.

Conversely, if $\varepsilon^{1/2}$ remains below $(\varepsilon^{1/2})^*$ during the increase stage, the steady-state values do not evolve significantly; they are nearly frozen, and it is hard to estimate whether there is a compaction or a decompaction process, because the dynamics is very slow. This last branch is called ''irreversible'' and reflects the great metastability of the corresponding packings.

To summarize, there is a strong hysteresis effect which allows the maximum compaction rate to be reached by an $\varepsilon^{1/2}$ increase-decrease sequence. These observations are in very good agreement with the results of Nowak *et al.* [7]. In particular, Fig. 4 is to be compared to the experimental data obtained with 1-mm-diameter beads, corresponding to an aspect ratio of nearly 19, close to that used in our simulation ($L/2R=16$). Surprisingly, for an aspect ratio of 9, the experimental results show a much larger increase of the packing fraction on the reversible branch, up to nearly 66% (i.e., more than the R.C.P. limit, which may indicate a commensurability between the cylinder and the beads [7]). However, for a still smaller aspect ratio of 6, the reversible branch is more similar to the first case, with a moderate increase to a maximal value below the 64% limit.

C. Aging

In these kinds of systems, in slow evolution to a final equilibrium, it is possible to demonstrate aging effects by comparing the system at different ages. This comparison can be made by use of temporal correlation functions of global values (ρ,$\langle Z\rangle$, . . .) between the initial packing and the same packing after an evolution time t_W (waiting time). In this study we work with the following function:

$$A(t,t_W)=\overline{[\langle Z\rangle(t_W)-\langle Z\rangle(t+t_W)]^2}. \qquad (5)$$

Here $\overline{x}$ indicates the statistical average of x; that is, the mean

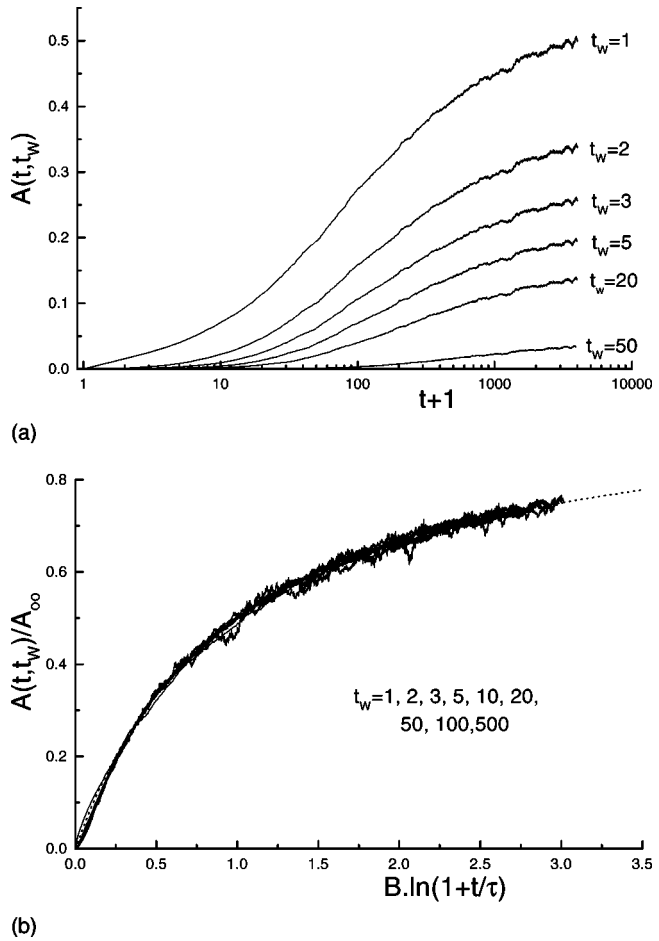

FIG. 5. Aging effects on the time-correlation function $A(t,t_W)$ for several waiting times t_W: the different curves (up), and a collapse according to the fit of the dotted line (down).

value calculated for a certain number of realizations of the same experiment. The results have been averaged on only ten realizations because of the limitation due to the calculation time. The statistics are, therefore, rather poor; that is why we use solely $\langle Z \rangle$, which fluctuates quite less than the other global values. In Fig. 5 we draw the curves of $A(t,t_W)$ obtained for different values of t_W. There is obviously a scaling law; a fit similar to that in Sec. III A, with the three parameters A_∞ (the asymptotic limit), B_A, and τ_A, is quite compatible with the data:

$$A(t,t_W)=A_\infty\left(1-\frac{1}{1+B_A\ln(1+t/\tau_A)}\right). \tag{6}$$

The same kind of aging effects were already pointed out in previous numerical studies [10,11]. These effects confirm the great similarity between granular compaction, or more generally slow granular rheology and glassy systems submitted to time-dependent driving forces (see, for instance, Refs. [21–23]).

To conclude with a global analysis of the compaction, it is satisfying to note that our simulation reproduces qualitatively well the previous results obtained both experimentally and theoretically. This model seems to capture most of the physics of the problem. Because it gives a very realistic description of a granular system such as a three-dimensional packing of hard spheres, it can be a quite useful and interesting tool to go beyond a global description to a local analysis of the packing's structure during the compaction process.

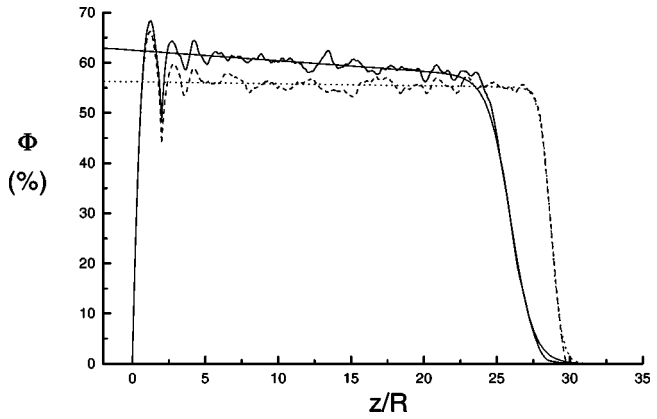

FIG. 6. Two examples of vertical density profiles with their fit: for the initial packing (dotted line), and for a packing obtained after 4000 taps with $\varepsilon=10^{-1}$ (solid line).

IV. LOCAL ANALYSIS

To study the packings of more or less compacted spheres locally, we use two kinds of descriptions: packing fraction (or density) profiles are calculated vertically and transversely to the box, and size and volume distributions of the pores in a packing are evaluated and then analyzed.

A. Density profiles

Using the surface packing fraction calculated by stereological cuts (as in the evaluation of Φ_b and $\langle \Phi^c \rangle$), we have access to vertical (horizontal cuts) and transverse (vertical cuts) density profiles. Some examples of vertical profiles are shown in Fig. 6. These have been obtained with F.B.C.'s, but the use of P.B.C.'s induces no significant differences. The profiles are characterized, in particular, by a negative vertical gradient α and by large peaks near the bottom of the box. These peaks reflect a partially ordered packing due to the wall, and are very close to previous experimental observations [24]. The gradient can be roughly estimated in an intermediate zone ($5 \leqslant z/R \leqslant 22$ for F.B.C.'s and $5 \leqslant z/R \leqslant 26$ for P.B.C.'s) after smoothing the profile. This gradient, directly linked to ε, is qualitatively different from previous numerical results [11], where a local densification was obtained at the interface. It could be objected that this gradient comes directly from a modeling of the tap through a uniform dilation. Nevertheless, despite the fact that α is difficult to estimate very precisely, it does not seem to be monotonic with $\varepsilon^{1/2}$, but has more or less the same kind of bell-shaped dependence as the other steady-state values. This behavior cannot be caused only by the dilation. However, in contrast to the other average values, it seems that α presents no hysteresis effect which denotes a relatively different behavior. In conclusion, the origin of the anisotropy of the packing, ob-

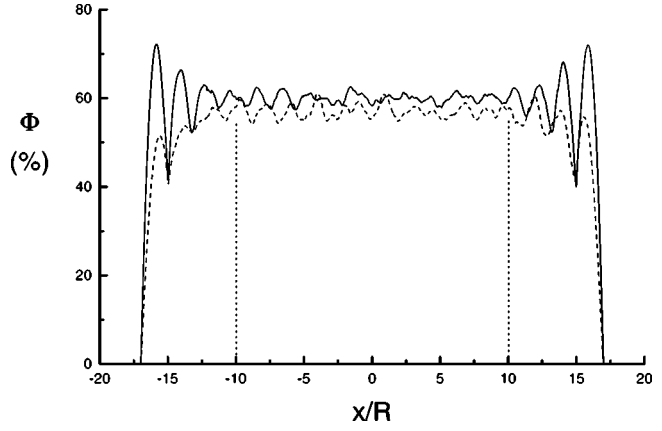

FIG. 7. Two examples of transverse density profiles: for the initial packing (dotted line), and for a packing obtained after 4000 taps with $\varepsilon = 10^{-1}$ (solid line). The two vertical dotted lines indicate the frontiers in the calculus of $\delta\Phi_{lateral}$ and $\delta\Phi_{central}$.

served through this gradient α, is not well understood. It may come from both the uniform dilation of the system and its specific redeposition under the simulated particle motion under gravity. Inspired by a Fermi level profile [25], we can propose the following average fit for a typical vertical profile:

$$\Phi(\bar{z}) = \frac{\Phi_0 - \alpha \bar{z}}{1 + \exp[\beta(\bar{z} - \bar{z}^*)]} \quad \text{where} \quad \bar{z} = z/R. \tag{7}$$

Figure 7 presents a few transverse profiles in fixed boundaries; they are qualitatively close to experimental profiles [26]. Here again, some peaks indicate a local organization in layers due to the walls; this effect has approximately a three-layer range. The average lateral density increase (at a distance less than $7R$ from the walls, corresponding roughly to this wall effects range) is noted as $\delta\Phi_{lateral}$, and the central increase as $\delta\Phi_{central}$. The last one is systematically smaller than the other. Both of these are calculated in comparison with the initial profiles, and reflect the spatial repartition of the bulk compaction. These profiles, with periodic boundaries, reveal no peak, due to the absence of walls. The central zone is a bit larger, but retains the same qualitative shape, and densifies during a tapping sequence. This observation of an obvious compaction even in P.B.C.'s ensures that compaction is not, or at least is not principally, due to wall effects. This was not evident when considering the small aspect ratio used in the experience of the Chicago group. Quantitatively, the absolute value of the packing fraction is larger in periodic conditions, but its increase due to compaction is a bit smaller.

As global values, $\delta\Phi_{lateral}$ and $\delta\Phi_{central}$ have the same dependence on $\varepsilon^{1/2}$ (bell shaped curves) as the others. It is also possible to study their evolution with the number of taps. The results, presented in Fig. 8, point out, once again, the nearly frozen dynamics for small values of $\varepsilon^{1/2}$.

Moreover, we can remark that the initial packing in F.B.C.'s presents a great metastability. This is particularly noticeable on the transverse profile (see Fig. 7), with an ''underpopulation'' of the spheres near the walls. This explains the significant compaction of $\delta\Phi_{lateral}$ caused by the first tap (see Fig. 8). This metastability is due to the construction of the initial packing: it was built by a gravitational algorithm [16] with periodic conditions, and a slight agitation was then induced in the packing to adapt it to fixed boundary conditions. This last stage was not sufficiently efficient.

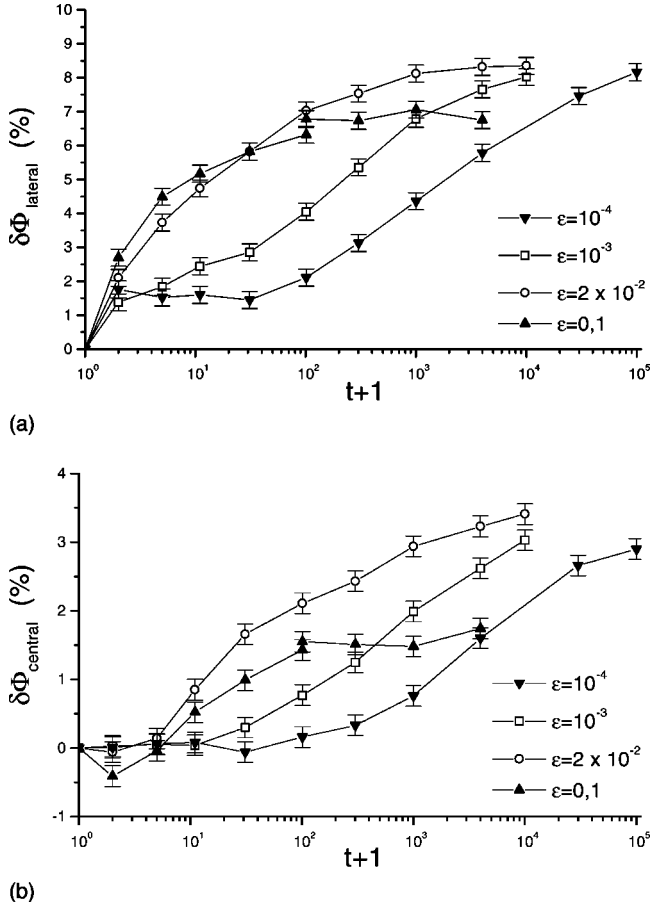

FIG. 8. Lateral (up) and central (down) packing fraction increases (in comparison with the initial packing) vs *t*, the number of taps for four values of ε.

B. Size and volume distributions of the pores

Another way to analyze the packing of particles is to study the interstitial voids. This void space is more difficult to apprehend because, in contrast to a particle, a cavity has no geometric limit. We then introduce the notion of pore as a ''void'' between four neighboring spheres. Previous studies were already made on this issue, both theoretically and experimentally. Gotoh *et al.* [27] introduced the pore size distribution P_0 as the probability for a randomly positioned sphere of radius r' to intercept no particle center. He proposed a theoretical expression for P_0 derived from the Percus-Yevick approximation which agrees well with previous results on random close packings [28,29],

$$0 \leqslant \sigma \leqslant 1, \quad P_0(\sigma) = 1 - \Phi\sigma^3, \tag{8}$$

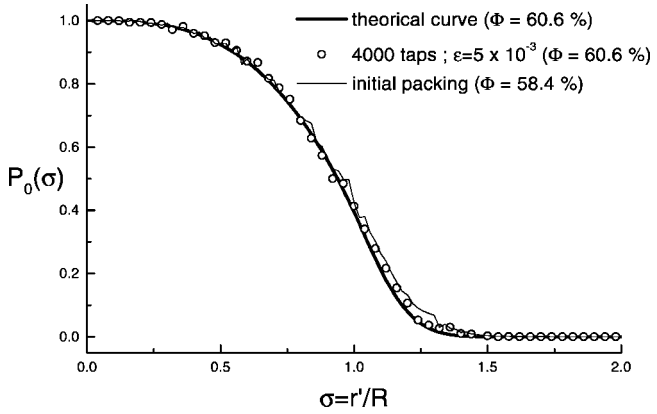

FIG. 9. Theorical pore size distribution P_0 (thick solid line) compared with the numerical calculation for a packing with the same average volume fraction (open circles). There is no significant difference from the calculations for the initial packing (thin solid line), which has a volume fraction this is quite a bit smaller.

$$1 \leqslant \sigma, \quad P_0(\sigma) = (1-\Phi)\exp\left[\frac{\Phi}{(1-\Phi)^2}[-(1-2\Phi)\sigma^3 + 9/2\Phi\sigma^2 + 1 - 5/2\Phi]\right], \tag{9}$$

where σ is the ratio r'/R (R is the radius of the hard spheres), and Φ is the average volume fraction. Figure 9 confronts this expression with a distribution calculated in one of the packings obtained after a compaction sequence of 4000 taps ($\Phi = 60.6\%$), and with periodic boundaries. The distribution calculated in the initial packing ($\Phi = 58.4\%$) is also represented, and is quite close to the other. This slight difference means that the distribution P_0 is insufficiently sensitive to small structural changes such as compaction.

Hence we find that it is more efficient to work with a direct statistical analysis on the size of the pores. To do this, we use the Voronoï tessellation of a packing [30]: a Voronoï polyhedon around a sphere is the region of space in which all the points are closer to this given sphere than to any other. Two neighbors correspond to two Voronoï polyhedra that share a face. Each vertex is equidistant from the center of four neighboring spheres, and therefore constitutes a pore. More precisely, we define the pore as a virtual sphere in contact with these four neighboring spheres, which interpenetrates none of them. The size of the pore is then the radius of this ''void sphere.'' The volume of this sphere partially reflects the total void volume situated inside the tetrahedron formed by the centers of the four neighboring spheres. In a packing, it is possible to calculate the size distribution of the pores $\rho_\xi(\xi)$, where $\xi = r/R$, with r the radius of a pore and R the radius of the hard spheres. The normalization gives $\int \rho_\xi(\xi) d\xi = N_P$, the total number of pores in the measurement volume. This distribution is linked to the previous one. Thus $P_0(\sigma = r'/R)$ is more or less the sum of the pores of size greater than r'. Therefore P_0 is a cumulative distribution in comparison with ρ_ξ, which is expected to be more sensitive to the local structure. A rather similar analysis by use of the size distribution of the pores was previously sketched out by Barker and Mehta [17].

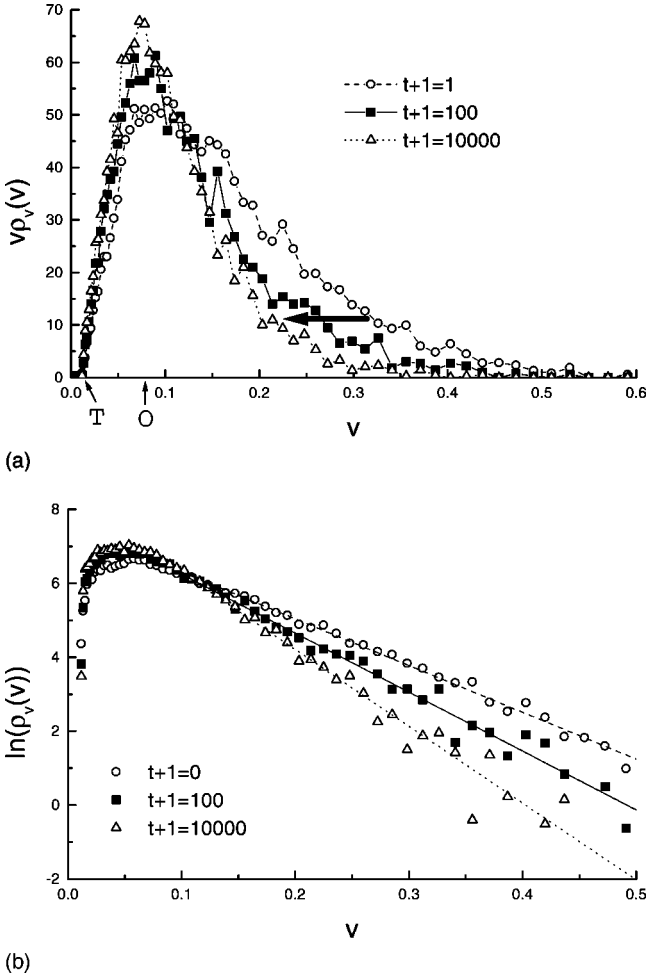

FIG. 10. (a) Volume distribution of the pores $v\rho_v(v)$ for a packing at different stages of its compaction (F.B.C.'s and $\varepsilon = 2 \times 10^{-2}$): $t+1 = 1$, 100, and 10 000. As the packing progressively densifies (i.e., as t increases), the tail of the distribution corresponding to the largest pores tends to vanish (as symbolized by the arrow). Here T and O indicate the v values for tetrahedral and octahedral sites in a dense packing (fcc or H.C.'s). (b) Plot of $\ln(\rho_v(v))$ vs v for the same packings. The different tails are compatible with a Poisson law.

If we now use directly the normalized volume $v = \xi^3 = 4/3\pi r^3/4/3\pi R^3$ as a new variable, the corresponding statistical density is $\rho_v(v) = (\xi/3)\rho_\xi(\xi)$ (here the ''volume'' of a pore is reduced to $4/3\pi r^3$). The distribution $v\rho_v(v)$ reflects the contribution of the pores to the total porosity according to their size; this last distribution seems to be more pertinent in problems of free volume and compaction. We have noted that, by integrating $v\rho_v(v)$, a new global value is obtained that corresponds to the average normalized volume of a spherical pore: $\nu = (1/N_P)\int v\rho_v(v)dv = \langle v \rangle / V$, where $\langle v \rangle$ is the average volume of a pore, V is the volume of the hard spheres, and N_P is the number of pores. The average pore volume ν has the same dynamics and the same kind of reversible-irreversible behavior as described in Sec. III B. Figure 10(a) shows the distributions $v\rho_v(v)$ for a given

TABLE I. Characteristics of the Bernal canonical holes.

	$\xi = r/R$	Number (%)	Volume (%)
tetrahedron	0.225	73.0	48.4
half-octahedron	0.414	20.3	26.9
trigonal prism	0.528	3.2	7.8
tetragonal dodecahedron	0.353	3.1	14.8
archimedian antiprism	0.645	0.4	2.1

packing at different stages of its compaction (in F.B.C.'s and with an excitation strength $\varepsilon = 2 \times 10^{-2}$). The statistics are calculated in a smaller box of height $18R$ located at a distance $2R$ from the walls to avoid some boundary problems. In this measurement volume, N_P varies approximately from 9550 to 10250 for the different packings analyzed. These different volume distributions $v\rho_v(v)$ are slightly affected by the taps in the small pore domain, whereas the variation of the packing fraction clearly appears in the progressive reduction of the tail of the distribution in the large pore zone. Thus, there is more or less a persistence of the distribution for values of v approximately limited by the volume of an octohedral site ($\xi_O = \sqrt{2} - 1 \approx 0.414$ and $v_O \approx 0.0711$). The distribution $v\rho_v(v)$ is bell shaped, with an overpopulation for the largest pores (the tail) and with a minimum size of the pores corresponding to a tetrahedral site ($\xi_T = \sqrt{3/2} - 1 \approx 0.225$ and $v_T \approx 0.0114$). With respect to the small pores, this is in contradiction with a Poisson distribution proposed in a previous theoretical model for logarithmic dynamics [31]. But, in Fig. 10(b), we note that, in a range of volume corresponding to the tail of the distribution, $\rho_v(v)$ is compatible with a Poisson law $\rho_v(v) \propto e^{(-v/v_0)}$, where v_0 is directly linked to ν, the average normalized volume already defined, or to $\langle \Phi^c \rangle$, the average packing fraction.

These results must be compared with previous work on the issue. First, Bernal [1] analyzed the arrangements of spheres by characterizing the cavities between the spheres. To do this, he studied the different polyhedra formed by the sphere centers as corner. He found five canonical holes. Table I [32] presents his results obtained on a mechanical model of hard spheres and concerning the statistical weight (in number and in volume) and the ξ value corresponding to each hole. In fact, these canonical holes are more or less distorted [otherwise $\rho_\xi(\xi)$ would be an addition of Dirac peaks], and the ξ value corresponding to the regular hole is therefore a lower limit. Thus we can note that the tetrahedron and the tetragonal dodecahedron correspond to the smallest values of ξ, for which we have shown that the volume distribution $v\rho_v(v)$ is not greatly affected by the tapping process. In contrast, the octahedron, the trigonal prism, and the archimedian antiprism (the two last in very low proportions) appear in the large pore range, and are consequently more sensitive to the compaction state of the packing. Thus, according to Bernal's classification on the structure of the pores, we can suggest that compaction is principally due to rearrangements of the three largest canonical pores.

V. CONCLUSIONS AND PERSPECTIVES

A simple model of hard spheres under vertical taps, based solely on geometric constraints is sufficient to describe previous experimental and numerical results qualitatively: the same kind of compaction dynamics, the same hysteresis effect on the steady-state values, and the same aging behaviors. The originality of this model, i.e., a realistic description of a granular system as a three-dimensional packing of hard spheres, permits a structural analysis of the packings. A semilocal study of density profiles suggests the existence of a negative vertical gradient in the packings but with no clear hysteresis effect. It also confirms a compaction in the bulk which cannot be caused only by wall effects, which are particularly noticeable with fixed boundaries (F.B.C.'s). A more local analysis on the void space of the packings shows, in a model of spherical pores, a volume distribution sensitive to the packing fraction for the large pores, that is nearly stationary for the small ones. Compaction could then be principally explained by collective rearrangements of the largest pores.

To further this numerical work, an experimental study of the compaction induced by vertical taps is being carried out. The packing fraction is deduced from a measure of absorption of a horizontal γ-ray beam. In addition to the average volume fraction in the bulk, our setup permits an evaluation of the vertical density profile in the packing; these measurements would be crucial in order to test the results of our numerical model, especially concerning the existence of a negative vertical gradient. Furthermore, compaction is studied in quite different experimental conditions than in the previous work of the Chicago group. In this later condition the setup is a tube of height 80 cm, with an approximate diameter of 2 cm filled with 1-mm-diameter soda lime glass beads. Thus, transverse wall effects are very significant, and the vertical pressure on the packing is saturated for almost the entire height of the heap, the overload being completely held up by the walls. Conversely, the cylinder used in our setup has a diameter of 10 cm and a height of 15 cm; about 80% of it is filled with 1-mm-diameter glass beads. Here the wall effects become negligible and the vertical pressure is definitely not saturated in the packing. It will be interesting to see to what extent these differences can qualitatively and quantitatively affect the compaction under vertical tapping.

ACKNOWLEDGMENTS

We are very grateful to R. Jullien for his support in numerical questions, especially concerning his gravitational deposition algorithm. We also wish to thank P. Richard, who constructed the program of size distribution of the pores, and J. Jenkins, who kindly read this manuscript and ran a spelling check on it.

[1] J. D. Bernal, Proc. R. Soc. London, Ser. A **280**, 299 (1964).
[2] H. M. Jaeger, S. R. Nagel, and R. P. Behringer, Rev. Mod. Phys. **68**, 1259 (1996).
[3] G. Y. Onoda and E. G. Liniger, Phys. Rev. Lett. **64**, 2727 (1990).
[4] J. G. Berryman, Phys. Rev. A **27**, 1053 (1983).
[5] G. D. Scott and D. M. Kilgour, J. Phys. D **2**, 863 (1969).
[6] J. B. Knight, C. G. Fandrich, C. N. Lau, H. M. Jaeger, and S. R. Nagel, Phys. Rev. E **51**, 3957 (1995).
[7] E. R. Nowak, J. B. Knight, M. L. Povinelli, H. M. Jaeger, and S. R. Nagel, Powder Technol. **94**, 79 (1997).
[8] E. R. Nowak, J. B. Knight, E. Ben-Naim, H. M. Jaeger, and S. R. Nagel, Phys. Rev. E **57**, 1971 (1998).
[9] E. Caglioti, V. Loreto, H. J. Herrmann, and M. Nicodemi, Phys. Rev. Lett. **79**, 1575 (1997).
[10] M. Nicodemi and A. Coniglio, Phys. Rev. Lett. **82**, 916 (1999).
[11] A. Barrat and V. Loreto, J. Phys. A **33**, 4401 (2000).
[12] P. L. Krapivsky and E. Ben-Naim, J. Chem. Phys. **100**, 6778 (1994).
[13] J. Talbot, G. Tarjus, and P. Viot, Phys. Rev. E **61**, 5429 (2000).
[14] S. F. Edwards and D. V. Grinev, Phys. Rev. E **58**, 4758 (1998).
[15] D. A. Head, Phys. Rev. E **62**, 2439 (2000).
[16] R. Jullien and P. Meakin, Europhys. Lett. **4**, 1385 (1987).
[17] G. C. Barker and A. Mehta, Phys. Rev. A **45**, 3435 (1992).
[18] E. Van Doorn and R. P. Behringer, Europhys. Lett. **40**, 387 (1997).
[19] L. Oger and J. P. Jernot, in *Disorder and Granular Media*, edited by D. Bideau and A. Hansen (North-Holland, Amsterdam, 1993).
[20] R. Ben Aim, Ph.D. thesis, Faculté des Sciences de l'Université de Nancy, 1970 (unpublished).
[21] L. Berthier, L. F. Cugliandolo, and J. L. Iguain, preprint, cond-mat/0010266.
[22] M. Sellitto and J. J. Arenzon, preprint, cond-mat/0006146.
[23] A. Barrat, J. Kurchan, V. Loreto, and M. Sellitto, preprint, cond-mat/0011492.
[24] R. F. Benenati and C. B. Brosilow, AIChE J. **8**, 359 (1962).
[25] H. Hayakawa and D. Hong, Phys. Rev. Lett. **78**, 2764 (1997).
[26] L. Vanel, Ph.D. thesis, Faculté des Sciences de l'Université de Paris VI, 1999 (unpublished).
[27] K. Gotoh, M. Nakagawa, M. Furuuchi, and A. Yoshigi, J. Chem. Phys. **85**, 3078 (1986).
[28] J. L. Finney, Proc. R. Soc. London, Ser. A **319**, 479 (1970).
[29] E. M. Tory, B. H. Church, M. K. Tam, and M. Ratner, Can. J. Chem. Eng. **51**, 484 (1973).
[30] P. Richard, Ph.D. thesis, Faculté des Sciences de l'Université de Rennes I, 2000 (unpublished).
[31] T. Boutreux and P. G. de Gennes, Physica A **244**, 59 (1997).
[32] H. J. Frost, Acta Metall. **30**, 889 (1982).